Progress In Electromagnetics Research B, Vol. 71, 137–152, 2016

Single Layered Wide Bandwidth Nanosized Strontium Hexa-Ferrite Filled LLDPE Absorber in X-Band

Soma Chakraborty[1], Nidhi Saxena Bhattacharyya[2], and Satyajib Bhattacharyya[1, *]

Abstract—A wide-band single-layer EMI shielding material for X-band is developed using an M-type strontium hexa-ferrite nanoparticle filler in LLDPE matrix. Strontium hexa-ferrite nanoparticles with crystalline size of 25.8 nm are obtained by annealing at 850°C. LLDPE allows a higher wt.% of ferrite inclusions enabling enhanced dielectric and magnetic losses. A peak absorption of 99.39% is achieved at 10.21 GHz when the filler weight in a 3 mm thick sample is adjusted to 60 wt.% while a wide −10 dB absorption bandwidth of 3.36 GHz centered around the same frequency is obtained. The density of the composite is 1.36 g/cm^3 and shows negligible water absorption.

1. INTRODUCTION

Magnetic absorbers are increasingly finding use in shielding of interfering electromagnetic waves. Permeability together with permittivity of the magnetic absorber results in impedance matching at the air-absorber interface ($Z' = \sqrt{\mu/\varepsilon}$), and also the thickness of the absorber decreases as the guide wavelength is reduced by a factor of $1/\sqrt{\mu\varepsilon}$. Magnetic losses along with dielectric losses enhance attenuation of the incident wave. Earlier magnetic absorbers used bulk ferrites and/or iron filings dispersed in matrix, mostly natural rubber, EPDM rubber, etc. [1, 2]. These absorbers were heavy and less resistant to corrosive environment [3]. Over the past decade, nano-sized magnetic materials have been increasingly used as inclusions for absorbers [4–7]. The reduced particle size splits the electronic energy level spacing which lies in the microwave range [8]. These discrete levels attenuate the impinging electromagnetic wave more rapidly as electrons absorb the energy when they move from one level to another.

Most of the applications require thin and light weight absorbers with wide absorption bandwidth. Multilayering and stacking are some of the methods for enhancing absorption bandwidth [9–11]. This, however, increases the thickness and weight of the absorber in addition to complicating the fabrication process. Single layered absorbers can be thin and light weight reducing any complexities in the structure and thus easing the fabrication process but inherently suffering from narrow absorption bandwidth [11, 12].

Absorbers are composites, generally made by dispersing filler particles homogeneously in different weight ratios in polymer matrix. The amount of inclusions in a composite is limited by percolation threshold of the polymer [13], thus, ceiling the value of permittivity and permeability of the composite and thereby the absorption. Generally, long side branched polymers such as polyvinylidene fluoride, polystyrene, novalac phenolic resin, etc. has lower percolation limit [13, 14]. Linear low density polyethylene (LLDPE) has a long linear chain and short side chain branching which disrupts the uniformity of the polymer thus preventing crystalline formation and permitting higher addition of filler percentage without making the composite brittle. LLDPE also has high tensile strength (18.8 MPa), low

Received 19 September 2016, Accepted 15 November 2016, Scheduled 29 November 2016

* Corresponding author: Satyajib Bhattacharyya (mwgece@gmail.com).

[1] Department of Electronics and Communication Engineering, Tezpur University, Assam 784028, India. [2] Microwave Engineering Laboratory, Department of Physics, Tezpur University, Assam 784028, India.

density (0.915 g/cm^3) and can be moulded easily into thin sheets. LLDPE is an inexpensive polymer with good resistance to chemicals [15–18]. M-type strontium hexagonal ferrite ($SrFe_{12}O_{19}$) is chosen as a filler in the present investigation because of its high anisotropy (anisotropy constant of 3.5×10^6 erg cm^{-3}), high saturation magnetization (74.3–92.6 emu/g), low density and high chemical stability [19, 20]. High resistivity of the hexagonal ferrite results in a higher dielectric loss while the resonance absorption of moving magnetic domains and spin relaxation at high-frequency electromagnetic field enhances magnetic loss [21–23].

Nano-sized strontium ferrite is synthesized using co-precipitation technique for use as magnetic filler. XRD analysis is carried out to determine the crystalline size. Composites with different wt.% of filler in LLDPE matrix are fabricated and homogeneity of distributions is ascertained from SEM images. Complex permittivity and permeability at microwave frequency of the composite is measured using the Nicolson-Ross method [24]. Other relevant characteristics for absorbers like saturation magnetization, water absorbance and density are also investigated. A single-layer absorber is designed using the transmission line model. The thickness of the single-layer absorber is optimized so as to achieve good impedance matching and obtain maximum absorption. Reflection loss of the fabricated single-layer absorber is measured in the X-band.

2. EXPERIMENTAL PROCEDURES

2.1. Synthesis of M-Type Strontium Ferrite ($SrFe_{12}O_{19}$)

Strontium nitrate ($\geq$ 98% purity, Merck) and iron (III) nitrate nonahydrate ($\geq$ 98% purity, Merck) precursors are used as the base materials to prepare M-type strontium ferrite ($SrFe_{12}O_{19}$) particles. The molar ratio of strontium nitrate to ferric nitrate is taken as 1 : 12. NaOH is added dropwise to control the size of the particles. Oleic acid is used as surfactant in order to reduce inter-particle interaction and prevent agglomeration. Aqueous solutions of strontium and iron salts are prepared separately by dissolving the salts in stoichiometric proportion in minimum amount of deionized water (0.1 M in 100 ml). The precipitate formed is then washed with a mixture of distilled water and ethanol to remove the sodium and nitrate compounds followed by drying to remove moisture. The dried powder is then annealed at a fixed temperature for 2 hours. Samples are prepared at three different annealing temperatures, 650°C, 750°C and 850°C to get three different samples of strontium ferrite powder. X-ray diffraction of the strontium ferrite prepared at three annealing temperatures is carried out to determine the crystalline size of each sample.

2.2. Composite Preparation ($SrFe_{12}O_{19}$-LLDPE)

LLDPE powder is sieved to get powder with particle size of $\leq 5\,\mu$m. Composite specimens of different wt.% are prepared by mechanically blending this sieved LLDPE powder with $SrFe_{12}O_{19}$ powder for about an hour. The mixture is then put into the die mould and cured for 2 hours by heating up to 110°C at a constant pressure of 36.5 MPa. Then, it is allowed to cool at room temperature.

A series of composite samples are prepared with increasing wt.% from 10 wt.% to 70 wt.% in steps of 10 wt%. Beyond 70 wt.%, the composite becomes brittle and hence not considered in this study. The composite is molded into pellets of dimensions 10.38 mm $\times$ 22.94 mm $\times$ 4 mm for microwave characterization.

3. CHARACTERIZATIONS

3.1. Microstructural Characterizations

X-ray diffraction (XRD) patterns (Rigaku, Miniflex 200 X-ray diffractometer) of the prepared filler materials are obtained using monochromatic Cu Kα radiation (wavelength, $\lambda = 1.541841$ Å) at room temperature over a 2θ angle from 20° to 70°. The value of lattice parameters are computed using d-spacing value and respective (h k l) parameters. Inter-planar distance, d is given by

$$\frac{1}{d^2} = \frac{4}{3}\left(\frac{h^2 + k^2 + l^2}{a^2}\right) + \frac{l^2}{c^2} \tag{1}$$

From the most prominent peaks, the average crystalline size (D) is calculated using Debye-Scherrer's equation

$$D = \frac{k'\lambda}{\beta \cos\theta} \tag{2}$$

where, k' is the Scherrer's constant and β the full width at half maximum (FWHM) of the particular peak.

Scanning electron microscope (SEM) studies are conducted with JEOL-JSM-6390 on the fabricated ferrite-polymer composite to find the homogeneous filler distribution in the host matrix.

3.2. Density and Water Absorbance

Density of a material gives an idea about the compactness of the material. Density measurement of the $SrFe_{12}O_{19}$-LLDPE nano-composite samples is carried out using Archimedes' principle. High moisture or humidity conditions can alter the material properties which can affect the absorber performance. The sample is tested for water absorbance by soaking in water for 72 hours at room temperature. Thereafter the samples are pat-dried. The weight of the sample is measured before and after soaking and % of water absorbed is calculated.

3.3. Saturation Magnetization

The magnetic field (B) or magnetic induction is given by (in cgs units)

$$B = H + 4\pi M_s \tag{3}$$

where, M_s is the magnetization produced when magnetic field H is applied to the material.

In S.I. units,

$$B = \mu_0(H + M) \tag{4}$$

Magnetization properties of the nano-composites are studied at room temperature using Pulsed Field Magnetometer developed at RRCAT, Indore. The saturation magnetization measurements are carried out for $SrFe_{12}O_{19}$-LLDPE composites. The applied field is 2.5 kOe.

3.4. Microwave Characterization

Complex permittivity and complex permeability over the X-band are computed from S_{11} and S_{21} values by Nicolson-Ross method. S_{11} and S_{21} parameters are measured using the transmission/reflection method, using an Agilent E8362C Vector Network Analyzer connected to an Agilent WR-90 X11644A rectangular waveguide line and the data acquired via an interfaced computer. The system is calibrated using thru-reflect-line (TRL) technique [25] before taking the measurements.

4. RESULTS AND ANALYSIS OF CHARACTERIZATIONS

4.1. X-Ray Diffraction of Strontium Ferrite ($SrFe_{12}O_{19}$)

Diffraction pattern of strontium ferrite annealed at 650°C, 750°C and 850°C is shown in Fig. 1. The diffraction peaks at 2θ values of 30.34°, 32.31°, 37.15°, 41.17°, 56.8°, 68.16° corresponds to the strongest diffraction planes (1 1 0), (1 0 7), (1 1 4), (2 0 5), (2 0 11), (2 2 0) and (2 0 14) and matches with those reported in JCPDS # 33-1340, indicating formation of $SrFe_{12}O_{19}$. The lattice constants, $a = 5.887$ Å and $c = 23.047$ Å determined from Eq. (1), correspond to hexagonal M type phase. The average crystalline size calculated from Eq. (2) is given in Table 1.

The crystalline size of strontium ferrite is in the nanometer range. The grain size of ferrite is observed to increase with increase in annealing temperature, a trait similar to that reported in [26, 27]. At the two lower sintering temperatures studied, i.e., 650°C and 750°C, additional diffraction peaks are observed at 25.14°, 43.52°, 49.48° and 54.09° corresponding to the planes (0 1 2), (2 0 2), (0 2 4) and (1 1 6) which is indexed to $Fe(NO_3)_3{\cdot}9H_20$ (JCPDS # 39-1346), showing presence of traces of precursors.

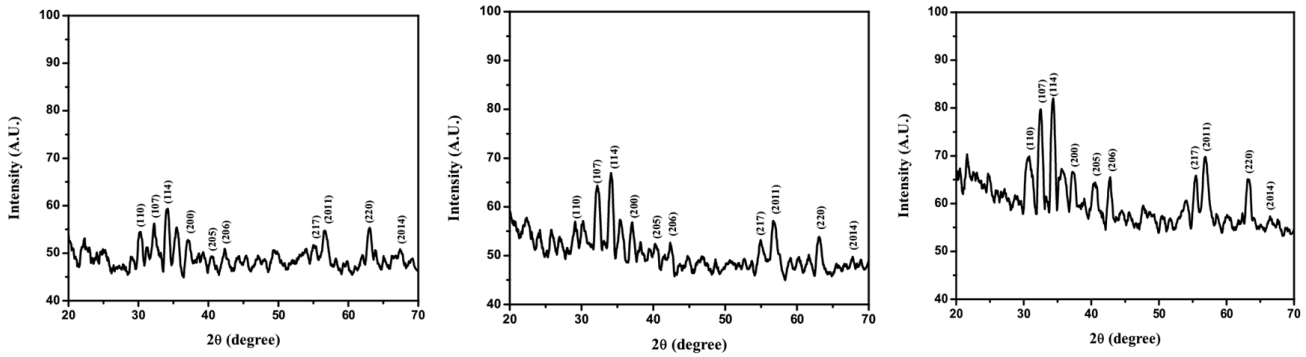

Figure 1. XRD pattern of $SrFe_{12}O_{19}$ annealed at (a) 650°C, (b) 750°C and (c) 850°C.

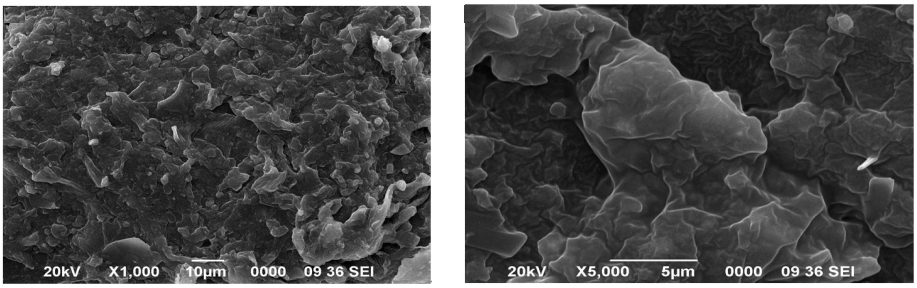

Figure 2. SEM images of 60 wt.% of $SrFe_{12}O_{19}$-LLDPE composite at magnification of (a) X 1000 and (b) X 5000.

Table 1. Calculated crystalline size (D) and lattice parameter of $SrFe_{12}O_{19}$.

Ferrite	Annealing temperatures	Average crystalline size, D (nm)	Lattice parameter, a (Å)	Lattice parameter, c (Å)
$SrFe_{12}O_{19}$	650°C	16.69	5.861	23.012
	750°C	24.27	5.875	23.031
	850°C	25.8	5.887	23.047

It is noteworthy that these peaks are absent at 850°C, showing complete annealing of the precursors. Composite samples with different wt.% of nanosized $SrFe_{12}O_{19}$ in LLDPE matrix is developed using strontium ferrite annealed at 850°C, hereafter referred to as $SrFe_{12}O_{19}$-LLDPE nano-composite.

4.2. Scanning Electron Micrograph

Scanning electron micrographs are taken at 10^{-11} A probe current and 20 kV accelerating voltage at different resolutions. Fig. 2 shows the SEM micrographs of 60 wt.% $SrFe_{12}O_{19}$-LLDPE nano-composite at different magnification. It is seen that there is no agglomeration of the filler particles in the matrix and more or less the distribution is uniform.

4.3. Density and Water Absorbance

Table 2 shows the density and water absorbance of 10 to 70 wt.% of $SrFe_{12}O_{19}$-LLDPE nano-composites. There is marginal increase in density of the nano-composite with increase in the ferrite content. The

composite shows negligible water absorption. The minimal increase water absorbance could be due to increase in porosity of the samples with increasing filler concentration.

4.4. Saturation Magnetization

The saturation magnetization values of the composites are given in Table 2. It is seen that saturation magnetization increases with increase in wt.% of the $SrFe_{12}O_{19}$ in LLDPE composite. The saturation magnetization of the composite is due to the net magnetic moment which depends on the wt.% of magnetic filler in the composite [28].

Table 2. Density, % water absorbance and saturation magnetization of $SrFe_{12}O_{19}$-LLDPE composite with varying wt. %.

wt. %	Density (g/cc)	Water absorbance (%)	Saturation magnetization (Tesla)
0 wt.%	0.93	0.01	...
10 wt.%	1.10	0.01	0.0084
20 wt.%	1.12	0.01	0.0090
30 wt.%	1.16	0.01	0.0099
40 wt.%	1.24	0.02	0.0106
50 wt.%	1.30	0.02	0.0117
60 wt.%	1.36	0.03	0.0128
70 wt.%	1.41	0.05	0.0193

4.5. Microwave Characterizations

4.5.1. Complex Permittivity and Permeability of $SrFe_{12}O_{19}$-LLDPE Composite with Different wt.%

Relative complex permittivity ($\varepsilon_r = \varepsilon'_r - j\varepsilon''_r$) and permeability ($\mu_r = \mu'_r - j\mu''_r$) measurements for all the wt.% of $SrFe_{12}O_{19}$-LLDPE nano-composite are carried out in the frequency range 8.2–12.4 GHz. ε'_r is the real part and ε''_r is the imaginary part of relative complex permittivity. μ'_r and μ''_r are real and imaginary part of relative complex permeability, respectively. The frequency plots of ε'_r and dielectric loss tangent, $\tan\delta_\varepsilon$ for different wt.% over the X-band is plotted in Figs. 3(a), (b) and does not show much variation with frequency. An increase in ε'_r from $\sim$ 3.8 to 6.4 and $\tan\delta_\varepsilon$ from 0.03 to 0.4 is observed as the amount of filler increases from 10 wt.% to 70 wt.%.

The frequency plots for μ'_r, and magnetic loss tangent, $\tan\delta_\mu (= \frac{\mu''_r}{\mu'_r})$ for 10 wt.% to 70 wt.% of $SrFe_{12}O_{19}$-LLDPE nano-composite is given in figures Figs. 3(c), (d). μ'_r and $\tan\delta_\mu$ shows a similar trend as for ε'_r and $\tan\delta_\varepsilon$, respectively, not showing much variation with frequency. With increase in filler content μ'_r increases from 0.98 to 1.26 while $\tan\delta_\mu$ changes from 0.003 to 0.142.

Polarization in ferrites is due to the presence of Fe^{2+} ions, with increase in the ferrite inclusions, concentration of Fe^{2+} ions increase and hence the net dielectric constant of the composite increases with increase in wt.% of the filler [27, 29]. The dispersion of complex permeability in a magneto-dielectric polymer composite is primarily due to the resonance of oscillating domain walls and the resonance of precessing magnetic moments in domains which is known as natural ferromagnetic resonance [21, 30]. However, in strontium the natural resonance peak lies at about 50 GHz [31]. For single domains, the domain wall oscillations are not present, but the crystallite size of strontium particles in this study is $\sim$ 25.8 nm, and hence the permeability of strontium can be attributed to the first phenomenon with increase in the weight percentage of $SrFe_{12}O_{19}$ in the composite the permeability increases accordingly. The high resistivity and high anisotropy [21] of strontium ferrite leads to higher values of dielectric and magnetic losses in the composite with higher filler percentage.

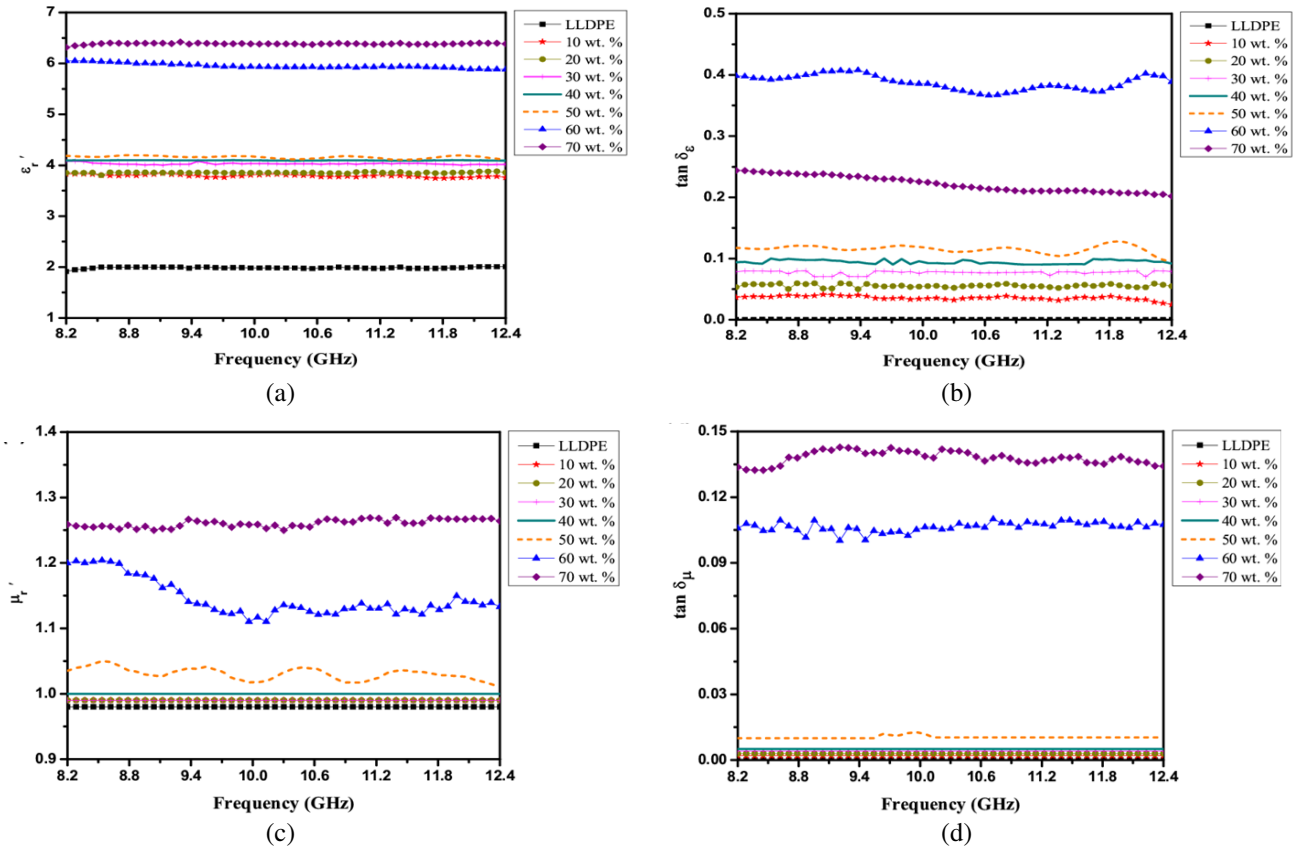

Figure 3. (a) Real part of complex permittivity (ε_r'), (b) Dielectric loss tangent ($\tan\delta_\varepsilon$), (c) Real part of complex permeability (μ_r'), (d) Magnetic loss tangent ($\tan\delta_\mu$) for 10 wt.% to 70 wt.% of $SrFe_{12}O_{19}$-LLDPE nano-composite.

4.6. Analysis of the Characterization

$SrFe_{12}O_{19}$-LLDPE nano-composites exhibit resonably high values of permittivity, permeability as well as both dielectric and magnetic losses, rendering them suitable for absorber design. The composite remains light weight as the density increases only marginally with increase in filler percentage up to 70 wt.%. Performance of absorbers using these nano-composites can be expected to be unaffected by moisture as water absorbance is found to be negligible. The nanosized strontium ferrite blends uniformly in LLDPE matrix assuring uniform propagation of electromagnetic wave in all directions. All the composites from 10 wt.% to 70 wt.% are designed and studied as reflection type single-layer absorbers using transmission line modeling [32] described in the following section.

5. DESIGN OF REFLECTION TYPE SINGLE-LAYER ABSORBER USING TRANSMISSION LINE MODEL

A schematic of a single-layer metal-backed absorber is shown in Fig. 4.

From Transmission Line Model (TLM), the reflection loss, RL, for a single-layer absorber is given by

$$RL = 20\log\left|\frac{Z_{in}-Z_0}{Z_{in}+Z_0}\right| \tag{5}$$

where, Z_{in} is the input impedance of the transmission line given by

$$Z_{in} = Z_0\frac{Z_R + Z_0\tanh\gamma\, t}{Z_0 + Z_R\tanh\gamma\, t} \tag{6}$$

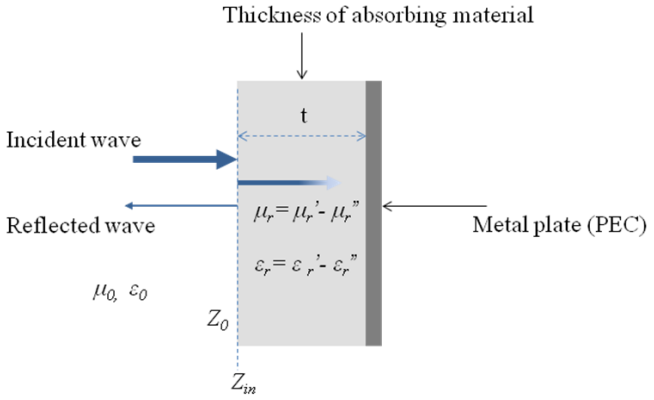

Figure 4. Schematic of a metal backed single-layer absorber.

$\gamma = j\frac{2\pi f}{c}\sqrt{\varepsilon_r \mu_r}$ being the propagation constant, t the thickness of the absorbing layer, Z_0 the characteristic impedance of free space and Z_R the impedance of the terminating load. For metal backing, $Z_R = 0$. Thus Eq. (6) becomes

$$Z_{in} = Z_0 \tanh\left[j\frac{2\pi f t}{c}\sqrt{\mu_r \varepsilon_r}\right] \tag{7}$$

where, f is the incident microwave frequency and c the velocity of light. Eq. (5) can be rewritten as

$$RL = 20 \log\left|\frac{\sqrt{\mu_r/\varepsilon_r}\tanh\left[(j2\pi f/c)\sqrt{\mu_r/\varepsilon_r}\, t\right] - 1}{\sqrt{\mu_r/\varepsilon_r}\tanh\left[(j2\pi f/c)\sqrt{\mu_r/\varepsilon_r}\, t\right] + 1}\right| \tag{8}$$

Absorption occurs if the reflection at the air-absorber interface is minimized, requiring $Z_{in} \to Z_0$. On entering the absorber, the wave attenuates exponentially within the absorbing material. The electromagnetic wave amplitude decays as $e^{-\alpha x}$, where x is the distance traversed by em wave inside the sample and α is the attenuation constant. The attenuation factor is determined from the expression [32]

$$\alpha = \frac{\sqrt{2}\pi f}{c} \times \sqrt{(\mu_r''\varepsilon_r'' - \mu_r'\varepsilon_r') + \sqrt{(\mu_r''\varepsilon_r'' - \mu_r'\varepsilon_r')^2 + (\varepsilon_r'\mu_r'' + \varepsilon_r''\mu_r')^2}} \tag{9}$$

Thus, from Eqs. (8) and (9), it is seen that effectiveness of microwave energy absorption depends upon the material parameters (complex permittivity, complex permeability, dielectric loss, magnetic loss), frequency of operation and the thickness of the absorber.

The reflection loss is optimized with thickness, t, of the composite using Eq. (8). Most of the strategic defense applications require thickness ≤ 4 mm [32]. Thus, the thickness of the absorber sample is varied from 1 mm to 4 mm in steps of 0.5 mm for 10 wt.% to 70 wt.% $SrFe_{12}O_{19}$-LLDPE nano-composites. Table 3 shows the calculated reflection loss (RL_c) values with varying thickness of the composite. Corresponding notch frequency (f_{Nc}), i.e., frequency at which the value of reflection loss is maximum is also included.

From Table 4 it is observed that 10 wt.% to 50 wt.% $SrFe_{12}O_{19}$-LLDPE nano-composite do not show significant reflection loss. 60 wt.% and 70 wt.% of $SrFe_{12}O_{19}$-LLDPE composite, however, show appreciable reflection loss. From Figs. 3(a)–(d), referring to the values of ε_r', μ_r' and loss tangent spectra, the real part of complex permittivity and permeability for these two weight fractions show higher values than rest of the compositions and the losses are also relatively high. As significant improvement in absorption is seen when the wt.% increases from 50 wt.% to 60 wt.%, samples with two in between wt.%, i.e., 55 and 65 wt.% are also fabricated and characterized. The real part of the complex permittivity, ε_r' and $\tan\delta_\varepsilon$ for 55, 60, 65 and 70 wt.% of the $SrFe_{12}O_{19}$-LLDPE nano-composite are plotted in Figs. 5(a), (b) over the X-band. The frequency plot of real part of the complex permeability, μ_r', and $\tan\delta_\mu$ for 55, 60, 65 and 70 wt.% of nano-composite is given in Figs. 5(c), (d).

Table 3. Calculated reflection loss (RL_c) of $SrFe_{12}O_{19}$-LLDPE with varying thickness and wt.% from 10 wt.% to 70 wt.% using TLM.

$SrFe_{12}O_{19}$-LLDPE	t (mm)	RL_c (dB)	f_{Nc} (GHz)
10 wt.%	1.0	-0.10	12.4
	1.5	-1.24	12.4
	2.0	-1.32	12.4
	2.5	-1.41	12.4
	3.0	-1.46	10.3
	3.5	-1.09	9.5
	4.0	-1.11	9.1
20 wt.%	1.0	-0.15	12.4
	1.5	-1.36	12.4
	2.0	-1.43	12.4
	2.5	-1.28	12.4
	3.0	-1.51	10.2
	3.5	-1.16	9.5
	4.0	-1.24	8.2
30 wt.%	1.0	-0.17	12.4
	1.5	-1.29	12.4
	2.0	-1.26	12.4
	2.5	-1.34	12.4
	3.0	-1.53	10.5
	3.5	-1.46	9.1
	4.0	-1.30	8.2
40 wt.%	1.0	-0.16	12.4
	1.5	-1.62	12.4
	2.0	-1.38	12.4
	2.5	-1.95	12.4
	3.0	-2.84	10.3
	3.5	-1.98	9.1
	4.0	-1.86	8.2
50 wt.%	1.0	-0.17	12.4
	1.5	-1.90	12.4
	2.0	-1.98	12.4
	2.5	-2.56	12.4
	3.0	-6.59	10.3
	3.5	-2.30	9.0
	4.0	-1.15	8.2
60 wt.%	1.0	-1.00	12.4
	1.5	-4.50	12.4
	2.0	-13.50	12.4
70 wt.%	1.0	-0.40	12.4
	1.5	-1.78	12.4
	2.0	-6.50	12.4
	2.5	-16.40	12.4
	3.0	-18.80	11.2
	3.5	-23.00	8.2
	4.0	-22.00	8.2

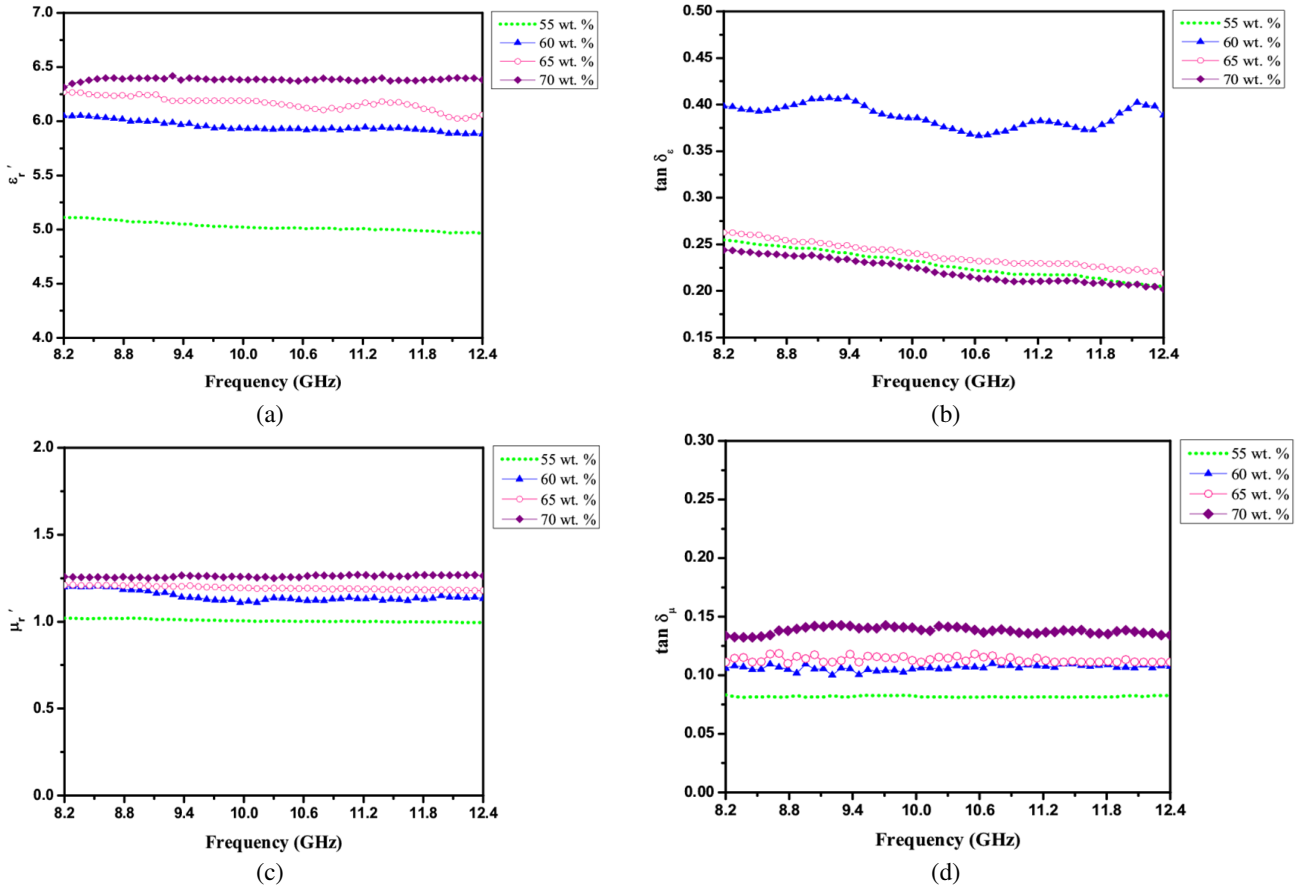

Figure 5. (a) Real part of complex permittivity (ε'_r). (b) Dielectric loss tangent ($\tan\delta_\varepsilon$). (c) Real part of complex permeability (μ_r). (d) Magnetic loss tangent ($\tan\delta_\mu$) for 55 wt.%, 60 wt.%, 65 wt.% and 70 wt.% of $SrFe_{12}O_{19}$-LLDPE nano-composite.

Table 4. Density, water absorbance and saturation magnetization of $SrFe_{12}O_{19}$-LLDPE with wt% varying from 55 wt.% to 70 wt.%.

$SrFe_{12}O_{19}$-LLDPE	Density (g/cc)	Water absorbance (%)	Saturation magnetization (Tesla)
55 wt.%	1.34	0.03	0.0117
60 wt.%	1.36	0.03	0.0128
65 wt.%	1.40	0.04	0.0162
70 wt.%	1.43	0.05	0.0193

The density, water absorbance and saturation magnetization values for the four compositions are given in Table 4.

Using Eq. (7), complex input impedance, Z_{in}, is calculated. Figs. 6–9 show the plots of real (Z'_{in}) and imaginary (Z''_{in}) values of input impedance. RL_c is determined using Eq. (8) for different thicknesses of the absorber for 55, 60, 65 and 70 wt.% composite over the X-band and Fig. 10 gives the values of RL_c for $SrFe_{12}O_{19}$-LLDPE composites with thickness varying from 1 mm to 4 mm. The results are tabulated in Table 5. Notch frequency, f_N, corresponding to the minimum value of RL is also included in the table.

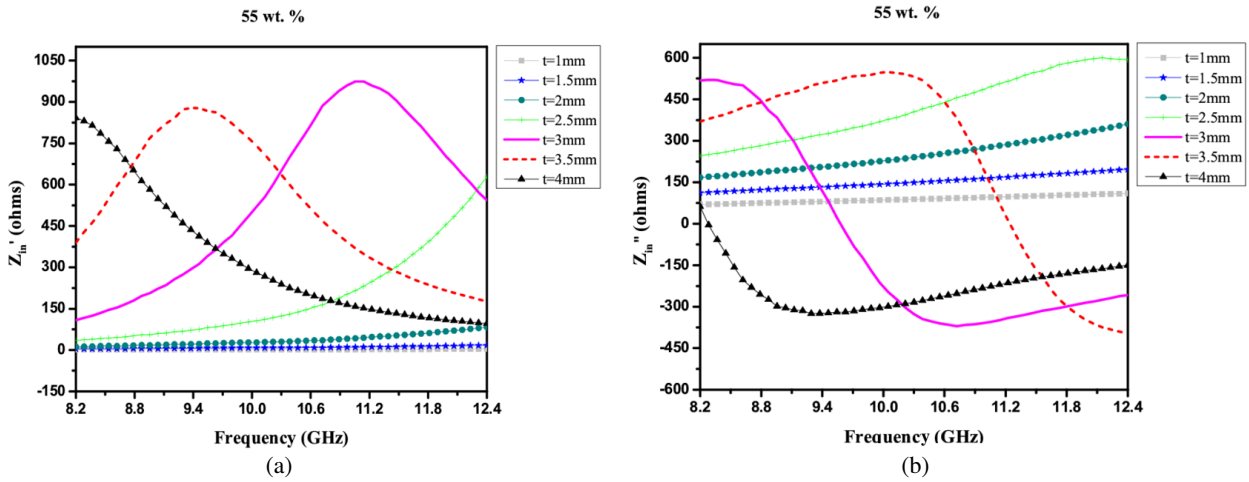

Figure 6. Calculated input impedance. (a) Real part of input Impedance (Z'_{in}). (b) Imaginary part of input Impedance (Z''_{in}) for $t = 1\,\text{mm}$ to $4\,\text{mm}$, 55 wt.% of $SrFe_{12}O_{19}$-LLDPE nano-composite.

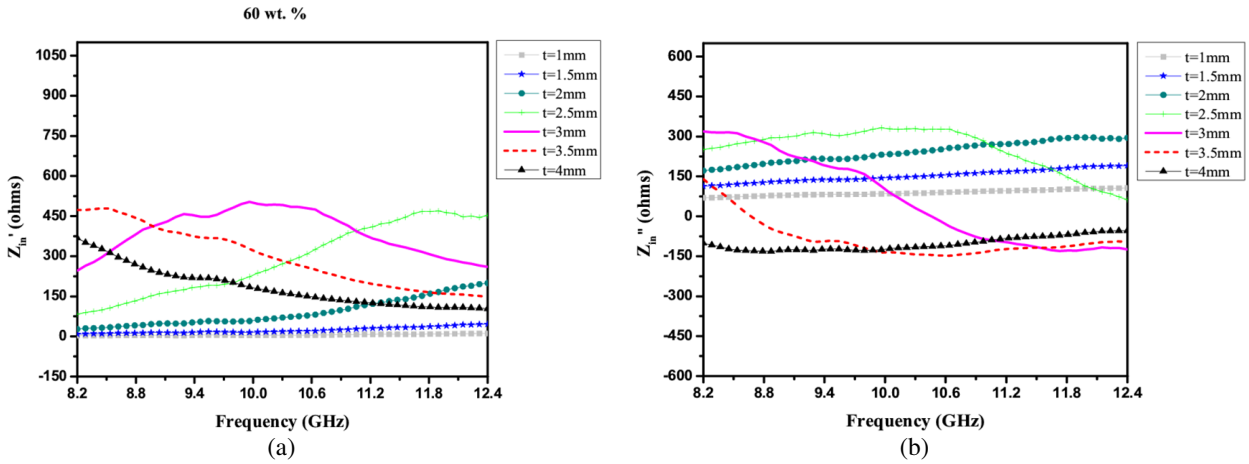

Figure 7. Calculated input impedance. (a) Real part of input impedance (Z'_{in}). (b) Imaginary part of input impedance (Z''_{in}) for $t = 1\,\text{mm}$ to $4\,\text{mm}$, 60 wt.% of $SrFe_{12}O_{19}$-LLDPE nano-composite.

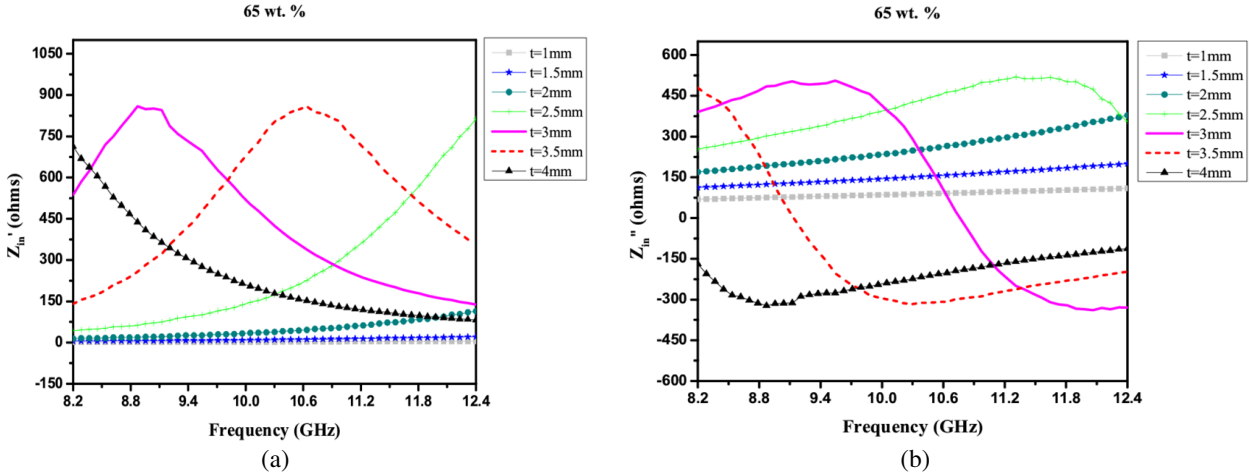

Figure 8. Calculated input impedance. (a) Real part of input impedance (Z'_{in}). (b) Imaginary part of input impedance (Z''_{in}) for $t = 1\,\text{mm}$ to $4\,\text{mm}$, 65 wt.% of $SrFe_{12}O_{19}$-LLDPE nano-composite.

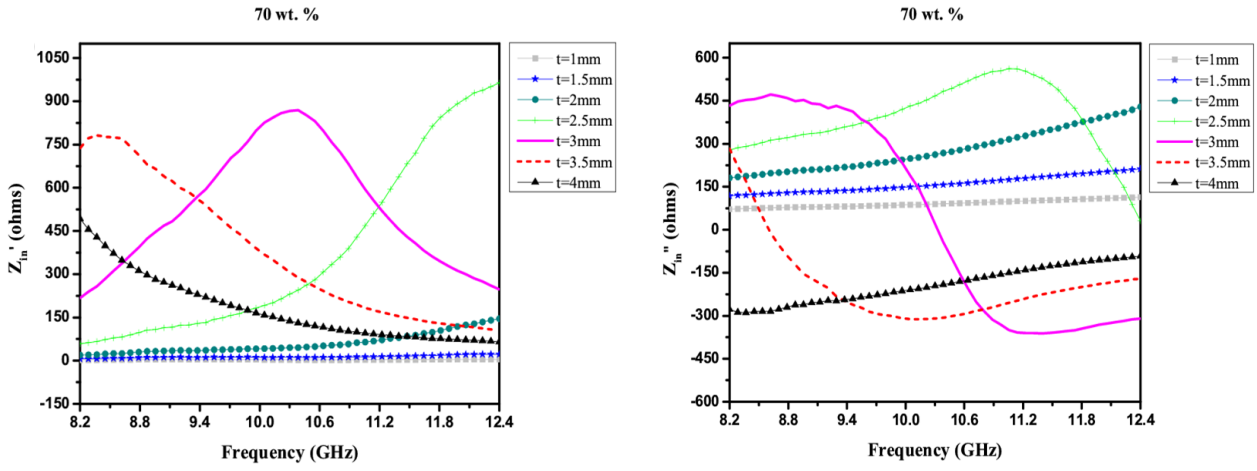

Figure 9. Calculated input impedance. (a) Real part of input impedance (Z'_{in}). (b) Imaginary part of input impedance (Z''_{in}) for $t = 1$ mm to 4 mm, 70 wt.% of $SrFe_{12}O_{19}$-LLDPE nano-composite.

Table 5. Input impedance, RL_c, -10 dB absorption bandwidth and f_{Nc} with varying thickness for 55, 60, 65 and 70 wt.% of $SrFe_{12}O_{19}$-LLDPE. (Calculated)

$SrFe_{12}O_{19}$-LLDPE	t (mm)	$Z_{in}'(\Omega)$	$Z_{in}''(\Omega)$	RL_c (dB)	f_{Nc} (GHz)	-10 dB BW_c (GHz)
55 wt.%	1.0	3.82	109.78	-0.37	12.40	-
	1.5	17.21	200.00	-1.42	12.40	-
	2.0	82.73	390.20	-4.55	12.40	-
	2.5	628.30	600.62	-11.88	12.40	0.58
	3.0	380.20	-200.24	-17.08	9.37	4.20
	3.5	257.41	-237.60	-16.40	11.07	2.64
	4.0	690.40	-380.54	-20.85	8.87	2.90
60 wt.%	1.0	11.04	106.33	-1.09	12.40	-
	1.5	50.00	205.20	-3.85	12.40	-
	2.0	200.23	308.30	-12.62	12.40	0.58
	2.5	450.48	92.41	-39.40	12.40	3.36
	3.0	440.32	-1.91	-39.70	10.30	4.20
	3.5	402.34	-67.63	-48.60	8.87	3.52
	4.0	390.64	-101.06	-39.00	8.20	4.20
65 wt.%	1.0	4.42	109.20	-0.43	12.40	-
	1.5	20.94	200.46	-1.73	12.40	-
	2.0	114.64	383.45	-5.92	12.40	-
	2.5	813.48	355.65	-15.83	12.40	1.43
	3.0	264.08	-190.78	-19.71	9.54	4.20
	3.5	708.86	-244.78	-20.00	11.39	3.40
	4.0	713.34	-169.08	-20.70	8.20	3.17
70 wt.%	1.0	4.10	113.13	-0.40	12.40	-
	1.5	22.11	212.02	-1.78	12.40	-
	2.0	145.78	410.73	-6.50	12.40	-
	2.5	964.43	230.83	-16.40	12.40	1.60
	3.0	487.70	-260.00	-18.80	11.39	4.10
	3.5	737.65	282.45	-23.00	9.20	3.78
	4.0	520.22	-277.90	-22.00	8.20	2.90

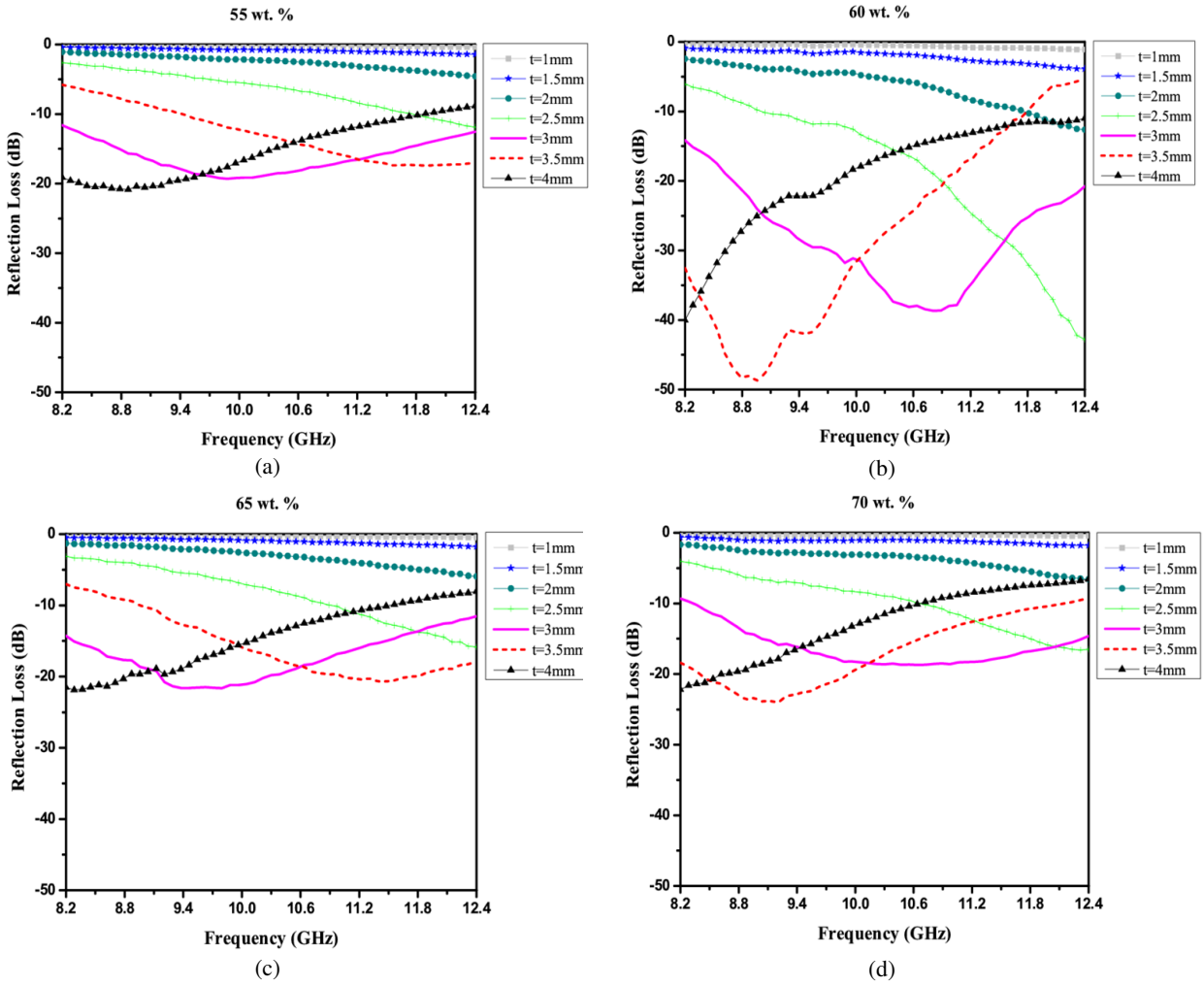

Figure 10. RL_c of $SrFe_{12}O_{19}$ LLDPE composite with thickness varying from 1 mm to 4 mm. (a) 55 wt.%, (b) 60 wt.%, (c) 65 wt.% & (d) 70 wt.% in X band frequency range. (Calculated)

From the plots in Fig. 10, it is observed that the −10 dB calculated absorption bandwidth (BW_c) is better for $t \geq 2.5$ mm for all wt.% as compared to those for $t < 2.5$ mm. 60 wt.% composites with $t = 3$ mm shows maximum −10 dB absorption bandwidth as well as peak RL value. It is interesting to see that the corresponding real (Z'_{in}) and imaginary (Z''_{in}) values of the input impedance are together closest to the free space real and imaginary impedance values of 377 Ω and 0 Ω, respectively, for all the wt. percentages (highlighted in Table 5) that are fabricated.

6. EXPERIMENTAL STUDY OF REFLECTION LOSS

Single-layer sheets of thickness $t = 3$ mm and dimension 10.38 mm × 22.94 mm are fabricated using $SrFe_{12}O_{19}$-LLDPE composites with wt.% of 55, 60, 65 and 70. The sample is placed inside an X-band sample holder (WR-90 X11644A) of length 97.8 cm mounted on the zero reference plane terminated by a short. S_{11} parameter is measured in the frequency range of 8.2–12.4 GHz. The measured reflection loss (RL_m) spectrum and calculated reflection loss (RL_c) using TLM for the same thickness $t = 3$ mm, for 55, 60, 65 and 70 wt.% composites in the X-band is given in Fig. 11.

The measured and calculated values of reflection loss, notch frequency and −10 dB absorption bandwidth are given in Table 6. From the table, it can be seen that 60 wt.% composite shows maximum RL_m of −22 dB and −10 dB absorption bandwidth (BW_m) of 3.36 GHz (8.536 GHz–11.896 GHz),

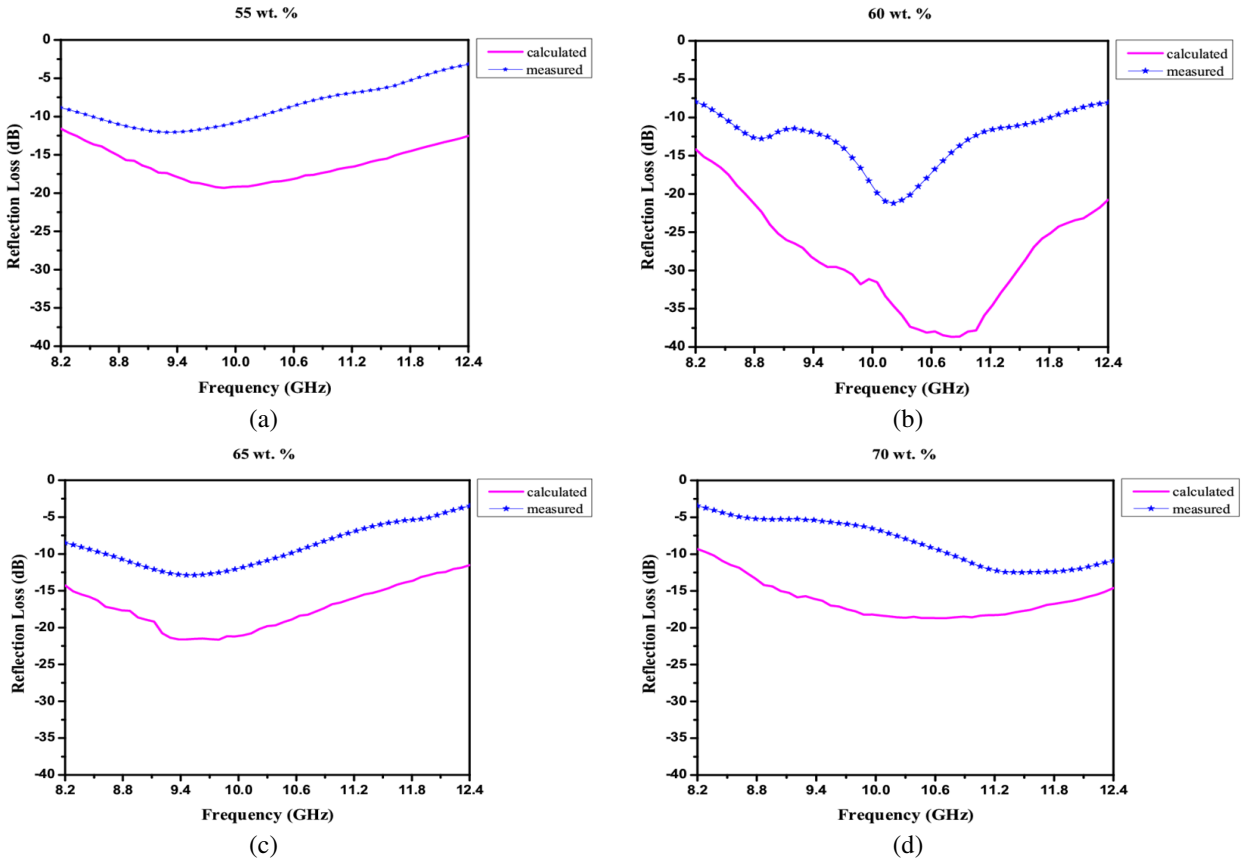

Figure 11. Measured and calculated RL of $SrFe_{12}O_{19}$ LLDPE composite with thickness $t = 3$ mm (a) 55 wt.%, (b) 60 wt.%, (c) 65 wt.% & (d) 70 wt.% in X band frequency range.

amongst all the wt.%, covering almost the entire X-band. The notch frequency of RL_m and RL_c are in close proximity; the small shift in frequency could be due to fabrication tolerance. The transmission line model used to calculate reflection loss having its attendant approximations, gives loss estimations generally on the higher side as compared to measured results [26]. Practically, the absorber is designed for specific thickness satisfying the condition of destructive interference at a particular frequency. The designed thickness may not satisfy this condition over the entire X-band leading to lower measured -10 dB absorption bandwidth as compared to calculated. There are no reported experimental works on undoped strontium ferrite as filler in single-layer composite absorbers to the best of knowledge of the authors. However, there are some computed results [5, 6, 23] reporting a -10 dB bandwidth of around 2.6 GHz for a single-layer absorber thickness of 2.4 mm [6] in the X-band.

Table 6. RL, -10 dB absorption bandwidth and notch frequency for 55, 60, 65 and 70 wt.% of $SrFe_{12}O_{19}$-LLDPE for $t = 3$ mm.

$SrFe_{12}O_{19}$-LLDPE	Measured			Calculated		
	RL_m (dB)	f_{Nm}	-10 dB BW_m (GHz)	RL_c (dB)	f_{Nc}	-10 dB BW_c (GHz)
55 wt.%	-12.07	9.40	1.6	-17.08	9.80	4.2
60 wt.%	-22.19	10.50	3.3	-39.70	10.68	4.2
65 wt.%	-12.87	9.46	1.9	-19.71	9.54	4.2
70 wt.%	-12.48	11.30	0.6	-19.71	11.03	4.1

The absorbers developed and characterized in the work show actual bandwidth performance comparable to the computed results using undoped strontium fillers. In one of the reported works [26], dual experimental −10 dB absorption bandwidths of 1.04 GHz and 1.01 GHz are achieved experimentally for a single-layer 50 wt.% barium ferrite-NPR composite absorber.

6.1. Attenuation

The attenuation constant (α) of the $SrFe_{12}O_{19}$-LLDPE composite is determined using Eq. (9) from the measured complex permittivity (ε_r) and complex permeability (μ_r) values of the composites for X-band.

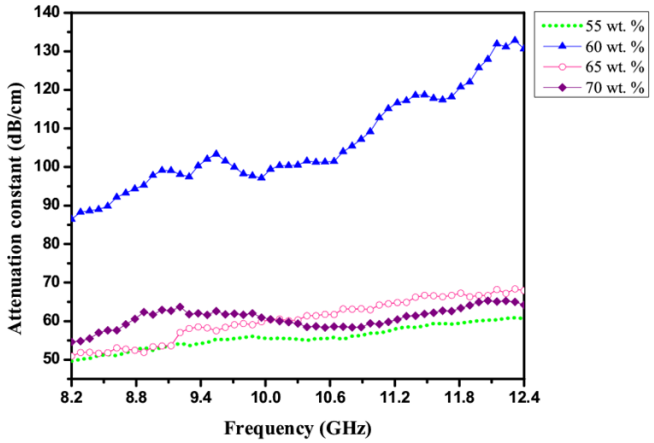

Figure 12. Attenuation constant of $SrFe_{12}O_{19}$-LLDPE for 55, 60, 65 and 70 wt.% and thickness, $t = 3$ mm in X-band.

Figure 12 shows the variation of attenuation constant with frequency. The maximum attenuation is obtained for the composite with 60 wt.% of $SrFe_{12}O_{19}$-LLDPE varying from 85.0 dB/cm at 8.2 GHz to 131.5 dB/cm at 12.4 GHz over the frequency range. The total loss is an aggregate of dielectric and magnetic losses [7]. In the 60 wt.% composite, the dielectric loss is higher than other compositions (Fig. 5(b)).

7. CONCLUSION

Nano-sized strontium ferrite is synthesized and included in LLDPE matrix in different weight ratios. Since LLDPE as matrix does not allow breakdown of the bonds, filler content up to 70 wt.% can be included in the matrix. A 3 mm thick single-layer composite of 60 wt.% $SrFe_{12}O_{19}$-LLDPE shows −10 dB absorption bandwidth of 3.36 GHz (8.536 GHz-11.896 GHz) and maximum attenuation. For higher absorption bandwidth, multilayered absorbers are studied. However, multilayering complicates the fabrication process and also increases the weight. In this case, the developed single-layer composite exhibits higher absorption bandwidth spanning almost the entire X-band which is preferable in broadband applications. This is achieved by using LLDPE as the matrix material, which allows a higher percentage of inclusions. Use of LLDPE also offers the added benefit of relatively lighter absorber weight and lower thickness. The prepared $SrFe_{12}O_{19}$-LLDPE absorber is resistant to water, and the lower density of nano magnetic fillers reduces the overall weight of developed composites. The performance of $SrFe_{12}O_{19}$-LLDPE composite validates its use as single-layer thin magnetic absorber in X band with improved absorption bandwidth.

ACKNOWLEDGMENT

This research did not receive any specific grant from funding agencies in the public, commercial, or not-for-profit sectors.

REFERENCES

1. Kim, S.-S., S.-T. Kim, Y. Yoon, and K. Lee, "Magnetic, dielectric, and microwave absorbing properties of iron particles dispersed in rubber matrix in gigahertz frequencies," *Applied Physics Letters*, Vol. 97, 10F905, 2005.
2. Annadurai, P., A. K. Mallick, and D. K. Tripathy, "Studies on microwave shielding materials based on ferrite and carbon black-filled EPDM rubber in the X-band frequency," *Journal of Applied Polymer Science*, Vol. 83, 145–150, 2002.
3. Verma, A., R. G. Mendiratta, T. C. Goel, and D. C. Dube, "Microwave studies on strontium ferrite based absorbers," *Journal of Electroceramics*, Vol. 8, 203–208, 2002.
4. Jalalia, M., S. Dauterstedt, A. Michaud, and R. Wuthrich, "Electromagnetic shielding of polymer–matrix composites with metallic nanoparticles," *Composites Part B Engineering*, Vol. 42, 1420–1426, 2011.
5. Vinayasree, S., M. A. Soloman, V. Sunny, P. Mohanan, P. Kurian, and M. R. Anantharaman, "A microwave absorber based on strontium ferrite–carbon black–nitrile rubber for S and X-band applications," *Composites Science Technology*, Vol. 82, 69–75, 2013.
6. Chen, N., G. Mu, X. Pan, K. Gan, and M. Gu, "Microwave absorption properties of $SrFe_{12}O_{19}/ZnFe_2O_4$ composite powders," *Material Science Engineering B*, Vol. 139, 256–60, 2007.
7. Koledintseva, M. Y., A. G. Razmadze, A. Y. Gafarov, V. V. Khilkevich, J. L. Drewniak, and T. Tsutaoka, "Attenuation in extended structures coated with thin magneto-dielectric absorber layer," *Progress In Electromagnetics Research*, Vol. 118, 441–459, 2011.
8. Ghasemi, A., V. Sepelák, X. Liu, and A. Morisako, "Microwave absorption properties of Mn–Co–Sn doped barium ferrite nanoparticles," *IEEE Trans. on Magnetics*, Vol. 45, 2456–2459, 2009.
9. Kim, K. Y., W. S. Kim, and S. Y. Hong, "A study on the behavior of laminated electromagnetic wave absorber," *IEEE Trans. on Magnetics*, Vol. 29, 2134–2138, 1993.
10. Komori, H. and Y. Konishi, "Wide band electromagnetic wave absorber with thin magnetic layers," *IEEE Trans. on Broadcasting*, Vol. 40, 219–222, 1994.
11. Motojima, S., Y. Noda, S. Hoshiya, and Y. Hishikawa, "Electromagnetic wave absorption property of carbon microcoils in 12–110 GHz region," *Journal of Applied Physics*, Vol. 94, 2325–2330, 2003.
12. Bregar, V. B., "Advantages of ferromagnetic nanoparticle composites in microwave absorbers," *IEEE Trans. on Magnetics*, Vol. 40, 1679–1684, 2004.
13. He, F., S. Lau, H. L. Chan, and J. Fan, "High dielectric permittivity and low percolation threshold in nanocomposites based on poly(vinylidene fluoride) and exfoliated graphite nanoplates," *Advanced Materials*, Vol. 21, 710–715, 2009.
14. Kakati, B. K. and D. Deka, "Differences in physico-mechanical behaviors of resol(e) and novolac type phenolic resin based composite bipolar plate for proton exchange membrane (PEM) fuel cell," *Electrochimica Acta*, Vol. 52, 7330–7336, 2007.
15. Saunders, K. J., *Organic Polymer Chemistry*, Chapman and Hall, 1973.
16. Domininghaus, H., *Plastic for Engineering*, Hanser Publishers, 1988.
17. Harper, C. A., *Handbook of Plastics Technologies*, McGraw Hill Professional, 2010.
18. Huang, X., F. Liu, and P. Jiang, "Effect of nanoparticle surface treatment on morphology, electrical and water treeing behavior of LLDPE composites," *IEEE Trans. on Dielectrics and Electrical Insulation*, Vol. 17, 1697–1704, 2010.
19. Cochardt, A., "Modified strontium ferrite, a new permanent magnet material," *Journal of Applied Physics*, Vol. 34, 1273–1274, 1963.
20. Guohong, M., N. Chen, X. Pan, H. Shen, and G. Mingyuan, "Preparation and microwave absorption properties of barium ferrite nanorods," *Material Letters*, Vol. 62, 840–842, 2008.
21. Ghasemi, A., A. Hossienpour, A. Morisako, A. Saatchi, and M. Salehi, "Electromagnetic properties and microwave absorbing characteristics of doped barium hexaferrite," *Journal of Magnetism and Magnetic Materials*, Vol. 302, 429–435, 2006.

22. Li, B. W., Y. Shen, Z. X. Yue, and C. W. Nan, "Influence of particle size on electromagnetic behavior and microwave absorption properties of Z-type Ba-ferrite/polymer composites," *Journal of Magnetism and Magnetic Materials*, Vol. 313, 322–328, 2007.
23. Ghasemi, A., X. Liu, and A. Morisako, "Effect of additional elements on the structural properties, magnetic characteristics and natural resonance frequency of strontium ferrite nanoparticles/polymer composite," *IEEE Trans. on Magnetics*, Vol. 45, 4420–4423, 2009.
24. Nicolson, A. M. and G. F. Ross, "Measurement of the intrinsic properties of materials by time-domain techniques," *IEEE Trans. on Instrumentation Measurement*, Vol. 19, 377–382, 1970.
25. Engen, G. F. and C. A. Hoer, "Thru-reflect-line: An improved technique for calibrating the dual six- port automatic network analyzer," *IEEE Trans on Microwave Theory and Techniques*, Vol. 27, 987–993, 1979.
26. Ozah, S. and N. S. Bhattacharyya, "Nanosized barium hexaferrite in novolac phenolic resin as microwave absorber for X-band application," *Journal of Magnetism and Magnetic Materials*, Vol. 342, 92–99, 2013.
27. Gupta, N., M. C. Dimri, S. C. Kashyap, and D. C. Dube, "Processing and properties of cobalt-substituted lithium ferrite in the GHz frequency range," *Ceramic International*, Vol. 31, 171–176, 2005.
28. Berkowitz, A. E., W. J. Shuele, and P. J. Flanders, "Influence of crystallite size on the magnetic properties of acicular γ-Fe_2O_3 particles," *Journal of Applied Physics*, Vol. 39, 1261–1263, 1968.
29. Verwey, E. J. W., "Electronic conduction of magnetite (Fe_3O_4) and its transition point at low temperatures," *Nature*, Vol. 144, 327–328, 1939.
30. Shin, J. Y. and J. H. Oh, "The microwave absorbing phenomena of ferrite microwave absorbers," *IEEE Trans. on Magnetics*, Vol. 29, 3437–3439, 1993.
31. Pullar, R. C., "Hexagonal ferrites: A review of the synthesis, properties and applications of hexaferrite ceramics," *Progress in Material Science*, Vol. 57, 1191–1334, 2012.
32. Feng, Y. B., T. Qiu, and C. Y. Shen, "Absorbing properties and structural design of microwave absorbers based on carbonyl iron and barium ferrite," *Journal of Magnetism and Magnetic Materials*, Vol. 318, 8–13, 2007.